

Stability analysis of a helium-filled thermoacoustic engine

W. Patrick Arnott,^{a)} James R. Belcher, Richard Raspet, and Henry E. Bass
Department of Physics and Astronomy, University of Mississippi, University, Mississippi 38677

(Received 19 August 1993; revised 9 March 1994; accepted 29 March 1994)

Spontaneous acoustic oscillations may occur in a sealed tube when an applied temperature gradient is larger than the temperature gradient associated with an acoustic standing wave in the tube. Work flow is the net acoustic power produced in the stack minus the net dissipated energy per cycle elsewhere. Instability occurs when the net work flow becomes a positive quantity. Recent theoretical results have shown that the thermoacoustic gain as well as the thermal and viscous losses can be expressed in terms of a thermoviscous dissipation function. The onset temperature and resonance frequency for a helium-filled thermoacoustic engine was computed using these theoretical results and measured as a function of the ambient pressure yielding stability and resonance frequency curves in good agreement. Expressions are derived using a short stack approximation for the optimal stack location and the onset temperature difference. These expressions are experimentally validated and are useful in searching for stack geometries that minimize the temperature difference across the stack necessary to deliver a given acoustic power.

PACS numbers: 43.35.Ud, 43.58.Bh

INTRODUCTION

Accounting for the departures from ideal, inviscid, adiabatic sound propagation is essential in order to correctly model sound in fluid-filled porous materials¹ and thermoacoustic engines.²⁻⁴ Sound in narrow capillary tubes is attenuated mainly by heat transfer and viscous drag at the tube wall. Though the acoustic wavelength is usually much greater than the tube diameter, thermal and viscous boundary layer thicknesses are often comparable to the diameter.

A common approach for the theory of sound in porous media is to envision the medium as a collection of capillary tubes. The generalization to capillary tubes of arbitrary geometry has recently been explored.¹ The equations and boundary conditions used in porous media modeling and in thermoacoustics are nearly identical (thermoacoustics has a very important extra term proportional to the ambient temperature gradient). Thermoacoustic gain and thermoviscous dissipation of sound in porous materials may be described theoretically with the use of a thermoviscous dissipation function.⁴ Viscous effects are then expressed as $F(\lambda)$, where λ is the shear wave number and thermal effects are expressed as $F(\lambda_T)$, where λ_T is the thermal disturbance number. The thermoviscous dissipation function $F(\epsilon)$ quantifies the exchange of momentum and heat between fluid and nearby solid walls through diffusion processes involving both fluid viscosity and thermal diffusivity and can depend strongly on the geometry of the perimeter between fluid and solid.⁴

We report on measurements and verification of the theoretical framework developed previously⁴ for the stability curve of a prime mover designed for the minimum onset temperature gradient. The system was designed to work on a frequency range such that by increasing the ambient pressure we could make the thermal boundary layer thickness span

the range from being larger than, to significantly smaller than the capillary tube diameters in the stack. The stack position was chosen by a preliminary numerical calculation to minimize the onset temperature difference necessary to produce enough net acoustic power in the stack to just overcome the acoustic power losses in the heat exchangers and resonator sections.

The amplitude of a pressure pulse in a circular tube normally decays in time (stable), but when a sufficiently large longitudinal temperature gradient is applied at the tube wall, the amplitude increases in time (unstable). Stability curves separate regions in operating parameter space, such as temperature gradient and ambient pressure, where on one side of the curve the system is stable, but is unstable on the other. Measurement^{5,6} and theory² of stability curves for circular tubes with temperature gradients were important in the early development of thermoacoustics. The present work extends stability curve analysis to pore shapes of current interest.³ It is shown that measured stability curves can be predicted accurately with current theory. The physics of the stability curve can be understood in terms of thermoacoustic power production in the stack and the dissipation of acoustic kinetic and potential energy per cycle both in the stack and elsewhere. Our results have application to the search for efficient prime movers and to the design of controlled acoustic resonators.

I. STABILITY CURVE MEASUREMENTS

Measurements of the onset temperature difference for self oscillation were performed on the thermoacoustic engine shown schematically in Fig. 1. The stack was the same square pore, porous wall, monolithic ceramic catalyst support characterized previously^{7,8} in association with sound propagation in air-filled porous materials. The heat exchangers are made of parallel copper strips (constructed as described previously^{9,10}). In Fig. 1, the variables are defined generally as follows: R is twice the pore area divided by the pore perimeter, L is the length of the section, and Ω is the

^{a)}W. Patrick Arnott is now at the Desert Research Institute, Atmospheric Sciences Center, P.O. Box 60220, Reno, NV 89506, and is an Adjunct Visiting Professor in the Department of Physics, University of Mississippi.

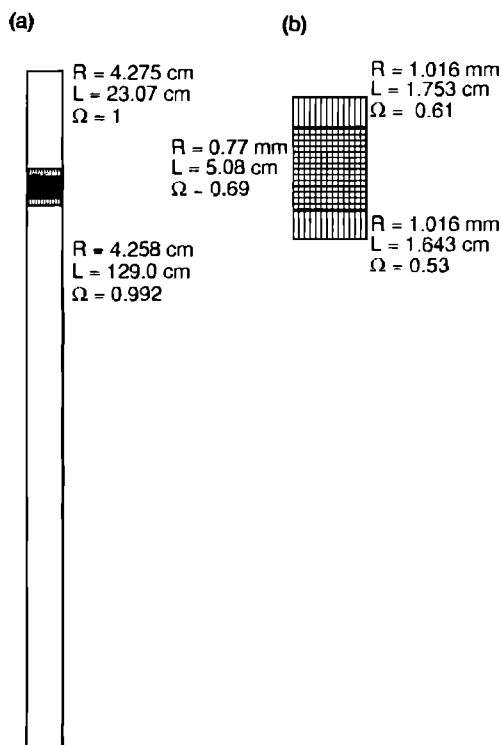


FIG. 1. (a) Scaled drawing and dimensions of the thermoacoustic engine and resonator. (b) Details of the heat exchangers (top and bottom) and engine.

porosity (the area of the open space between pores divided by the area of the cross section of the resonator tube section at the top). In the case of the resonator sections, R is just the tube radius.

The top heat exchanger and portion of the tube were heated by a resistance heater. The bottom heat exchanger and portion of the resonator were maintained at 20 °C with water circulated through a cold bath. Type K thermocouples embedded well into the heat exchangers were used to monitor temperature. The resonator was sealed against leaks and filled with helium. Gas was allowed to escape to maintain constant pressure as the top end was heated. The temperature at the top end was increased slowly until sustained self-oscillation was just detected. The temperature difference between the heat exchangers was then recorded along with the ambient pressure and frequency of operation. The tube was then cooled down, the ambient pressure changed, and the process was repeated. Measurements were performed for ambient pressures of 143, 170, 184, 198, 212, 239, and 308 kPa.

Measurements of the onset temperature difference between the hot and ambient heat exchangers $\Delta T \equiv (T_H - T_C)$, and resonance frequency, f_0 , as a function of the hot ambient pressure are shown in Fig. 2(a) and (b) as the crosses. The minimum in onset temperature is related to the thermal boundary layer thickness and to a lesser extent the position of the stack in the standing wave. Resonance frequency depends on ambient pressure through velocity dispersion in the tube and thermoacoustic elements and through the onset temperature because of heating of the gas column at the top of the tube.

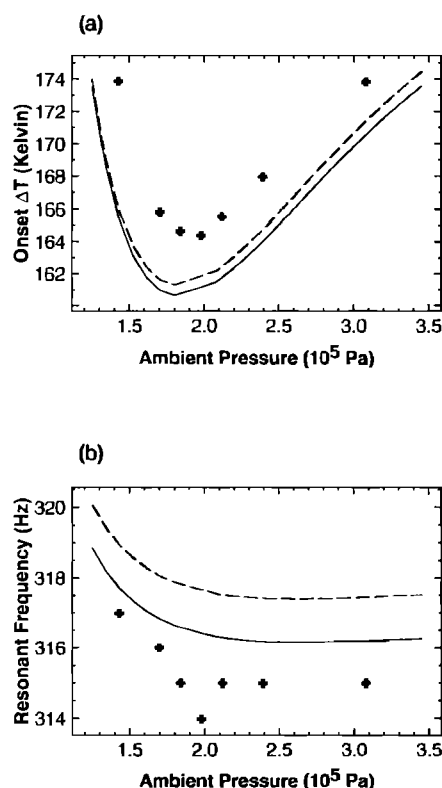


FIG. 2. (a) Onset or critical temperature and (b) associated resonance frequency versus the ambient pressure in the resonator. Experimental values are the crosses, solid (dashed) lines are porous wall (nonporous wall) stack calculations.

II. MODEL RESULTS FOR THE STABILITY CURVE

A general analysis scheme has been developed⁴ which utilizes impedance and pressure translation equations. The impedance and pressure at one end of a section is used to determine these quantities at the other end. The resonance frequency, onset temperature, phase angle of pressure at the stack, and work load at the ends of the stack can be determined using the impedance and pressure translation equations.

The specific acoustic impedance at the top of the hot end of the resonator in Fig. 1 is much greater than the characteristic impedance of the gas. The impedance at the top is calculated using boundary layer theory¹¹ which accounts for heat transfer to and from the compressed and expanded gas at the resonator cap. The specific acoustic impedance at the top of the hot heat exchanger and top of the stack are computed using Eq. (36) of Ref. 4. The same equation is used to compute the impedance from the bottom of the stack to the cap at the bottom of the ambient end of the resonator. Impedance in the thermoacoustic engine [the middle section in Fig. 1(b)] was computed using numerical integration of the first-order nonlinear differential equation given as Eq. (33) in Ref. 4. Acoustic pressure was assumed to be unity at the hot end cap, and was computed elsewhere using translation equations, Eq. (35) and Eq. (37) of Ref. 4.

The temperature in the stack was assumed to depend linearly on position. The ceramic stack was characterized previously.^{7,8} The material has walls that are porous which

tends to increase (decrease) the complex wave number (characteristic impedance) over that which a nonporous wall material of the same dimensions would have.⁸ The effects of finite wall porosity can be accounted for by using the complex wave number, k and characteristic impedance as described in Ref. 8.

An excited resonance evolves in time as $\exp(-i\omega_0 t)$ where the complex eigenfrequency is $\omega_0 \equiv 2\pi f_0 - i\pi f_0/Q$, with Q the quality factor, $i = (-1)^{1/2}$, and f_0 the resonance frequency.³ The pressure pulse exponentially decays for $Q > 0$, maintains as $Q \rightarrow \infty$, and grows exponentially, at least initially, for $Q < 0$. The complex eigenfrequency is determined by matching the impedance computed from use of the impedance translation equations with the impedance at the cap at the bottom of the resonator.⁹ Newton-Raphson iteration was used in the complex plane to determine the complex root, ω_0 . Starting values of ω_0 for iteration were determined by assuming a constant amplitude driver at the bottom of the resonator, and scanning frequency to determine resonance and half power bandwidth to determine Q . The onset temperature difference was determined by the condition $Q \rightarrow \infty$, or operationally, $1/Q \rightarrow 0$. It should be noted that the complex eigenfrequency approach accounts for power dissipation (and generation in the stack) everywhere in the resonator.

Results of the complex eigenfrequency calculation are shown in Fig. 2(a) and (b). The nonporous wall calculation (dashed line) predicts a higher operating frequency and hence more attenuation at the heat exchangers and resonator walls than does the porous wall calculation (solid line). Residual disagreement (less than 3%) between porous wall stack theory and experiment is probably due to the disregarded pressure drops and flow resistances between heat exchangers and the stack.

III. SHORT STACK APPROXIMATION FOR THE STABILITY CURVE

Work flow as computed from the short stack approximation^{3,4} will be used to derive the optimal position of a stack in the standing wave and the corresponding minimal onset temperature difference of the stack. The gas properties are assumed to be constant and are evaluated at the temperature at the hot end of the stack. The stack position and onset temperature depend on the work load the stack must deliver and the ratio of stack pore characteristic dimension R to thermal boundary layer thickness. We derive, for a given work load, an explicit expression for choosing stack position and R that give an optimally low value for the onset temperature difference of the stack.

A nondimensional critical temperature gradient can be defined:

$$\tau \equiv \frac{\beta(T_H - T_C)}{2k_0 d}, \quad (1)$$

where T_H (T_C) is the temperature above (below) the stack in Fig. 1(a), β = coefficient of thermal expansion ($\beta = 1/T$ for an ideal gas), $k_0 = 2\pi f_0/c$ is the adiabatic propagation constant for sound speed c and operating frequency f_0 , and d is the stack length. τ is a nondimensional measure of the tem-

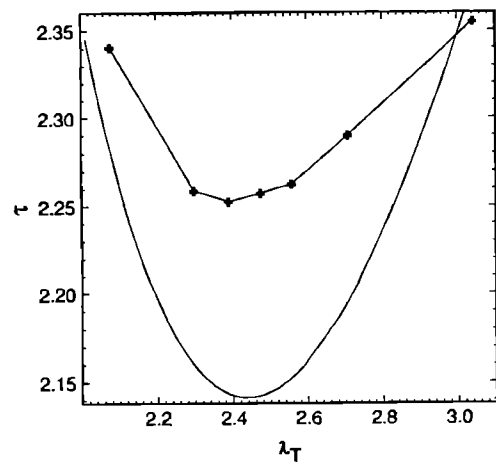


FIG. 3. Normalized onset temperature gradient against the thermal disturbance number. Experimental values are shown by crosses and are connected by lines for convenience. Theoretical values from the short stack approximation in Eq. (6) are given by the solid line.

perature gradient necessary for thermoacoustic power production to just match the sum of power dissipation elsewhere in the prime mover.

A better understanding of stability in the tube can be developed by plotting τ against the dimensionless thermal disturbance number in the stack. The horizontal axis is the nondimensional thermal disturbance number given by $\lambda_T = R(\rho_0 \omega c_p / \kappa)^{1/2}$ or $\lambda_T = 2^{1/2} R / \delta_\kappa$, which is the ratio of the square pore characteristic dimension $R = 0.77$ mm, to the thermal boundary layer thickness δ_κ . Use of the Prandtl number $N_{pr} = \eta c_p / \kappa$ ($= \frac{2}{3}$ for helium) gives the relation $\lambda_T = \lambda N_{pr}^{1/2}$, where $\lambda = R(\rho_0 \omega / \eta)^{1/2}$ is the dimensionless shear wave number. Density and heat capacity were computed from ideal gas relations. Viscosity was computed using $\eta = 1.887 \times 10^{-5} (T_0 / 273.15)^{0.6567}$ (mks units), where T_0 is the ambient temperature. Sound speed was computed using the ideal gas relation. The normalized onset temperature gradient is shown against λ_T in Fig. 3. The resonance frequency measurements (which were used to determine $\omega = 2\pi f_0$) were only accurate to within 1 Hz, though this in no way limits the general conclusions of the paper since a 1-Hz change of f_0 changes λ_T by less than one part in 100. The thermal boundary layer at the top end of the stack is $\delta_\kappa = 0.58 R_{\text{stack}} = 0.45$ mm at the minimum onset temperature gradient in Fig. 3 where $\lambda_T \approx 2.44$. The thermal boundary layer thickness is obviously an important length scale in thermoacoustics. The resonator length is the same order as the acoustic wavelength, and the thermoacoustic elements have pores with R the same order as the thermal boundary layer thickness.

A short stack approximation for τ will be derived. A standing wave is assumed with pressure, $p_1(z)$, and particle velocity, $v_2(z)$, at the upper end of the thermoacoustic engine given by

$$p_1(z) = p_1(0) \cos k_0 z, \quad (2a)$$

$$v_2^s(z) = \frac{p_1(0)}{\Omega \rho_0 c} \sin k_0 z, \quad (2b)$$

$$v_z(z) = iv_z^s(z), \quad (2c)$$

where the wave number in the empty tube is $k_0 = \omega/c$ and c is the sound speed in free space, Ω is the stack porosity, and z is the distance from the upper end. When z is less than one quarter of a wavelength, $p_1(z)$ and $v_z^s(z)$, are greater than zero. Denote by $V_G = A_{\text{res}}\Omega d$ the open volume of the stack (extending wall pores) where d is its length and A_{res} is its cross-sectional area. The net work flow produced in the stack (prime mover) to first order in $k_0 d$ is^{4,12}

$$\begin{aligned} \bar{W}_s(z) = & -\omega \frac{V_G p_1^2(z)}{2\rho_0 c^2} (\gamma-1) \text{Im} F^*(\lambda_T) \\ & -\omega \frac{\rho_0 V_G v_z^s(z)}{2} \frac{\text{Im} F^*(\lambda)}{|F(\lambda)|^2} \\ & + \frac{V_G}{2} p_1(z) v_z^s(z) \beta \frac{(T_H - T_C)}{d} \frac{\text{Im}\{F^*(\lambda_T)/F^*(\lambda)\}}{1 - N_{\text{pr}}}, \end{aligned} \quad (3)$$

where γ is the ratio of specific heats and β is the coefficient of thermal expansion. The first and second terms, always negative, are general expressions for dissipation of potential and kinetic energy per unit time due to thermal and viscous diffusion processes and it is applicable for arbitrary pore diameters and shapes. The third term, which is positive when the hot end faces a pressure antinode, is the acoustic power produced by the temperature gradient. When the third term is larger than the sum of the first two the stack produces net acoustic power. The amount of loss by thermal or viscous dissipation and gain by the thermoacoustic mechanism is weighted by the position of the stack in the standing wave. Thermal loss is minimized by placing the stack near a pressure node and viscous loss is minimized by placing the stack near a velocity node, but thermoacoustic gain is highest midway between these nodes. The thermoviscous dissipation function $F(\epsilon)$ appearing in Eq. (3) refers to thermal dissipation of sound for $\epsilon = \lambda_T$, and viscous dissipation when $\epsilon = \lambda$. This function has a central role in thermoacoustics. The function $F(\epsilon)$ generally has both real and imaginary components, depends strongly on stack geometry (e.g., square pores, parallel slits, circular pores, etc.) and the equations for different pore geometries along with the graphs are explored at length in Sec. II of Ref. 4. It should be noted that Eq. (3) is not a boundary layer approximation as given in Eq. (80) of Ref. 3, but contains the boundary layer approximation as a special

case with the use of the appropriate $F(\epsilon)$ given in Eq. (75) of Ref. 4. Thus Eq. (3) allows for evaluation of stacks having different pore geometries as discussed below.

Denote by \bar{W}_{ext} the total rate of work loss in the heat exchangers and the rest of the resonator. Oscillations can occur when

$$\bar{W}_s + \bar{W}_{\text{ext}} \geq 0. \quad (4)$$

It is useful to nondimensionalize \bar{W}_{ext} by defining

$$\bar{w}_{\text{ext}} \equiv \frac{2\rho_0 c^2 \bar{W}_{\text{ext}}}{p_1^2(0) V_G \omega} = \frac{2\gamma p \bar{W}_{\text{ext}}}{p_1^2(0) V_G \omega}. \quad (5)$$

The second form assumes an ideal gas and is independent of the ambient temperature.

The onset temperature gradient for the thermoacoustic engine can generally be evaluated using Eq. (1), Eq. (3), and Eq. (4). Evaluation of the onset condition in Eq. (4) gives

$$\begin{aligned} \tau = & \frac{\Omega(1 - N_{\text{pr}})}{\text{Im}\{F^*(\lambda_T)/F^*(\lambda)\}} \left(\frac{\bar{w}_{\text{ext}}}{\sin(2\phi)} \right. \\ & \left. + \frac{(\gamma-1)\text{Im} F^*(\lambda_T)}{2 \tan \phi} + \frac{\tan \phi \text{Im} F^*(\lambda)}{2|\Omega F(\lambda)|^2} \right). \end{aligned} \quad (6)$$

The phase angle and external work flow were computed (using the accurate calculations described in Sec. III) to be $\phi = k_0 z = 27.2$ deg and $\bar{w}_{\text{ext}} = 0.52$ for $\lambda_T \approx 2.4$. This is the value of λ_T corresponding to the minimum experimental onset temperature difference in Fig. 3. The short stack approximation Eq. (6) for τ is shown along with experimental data in Fig. 3, verifying the utility of the approximation. It should be noted that both ϕ and \bar{w}_{ext} depend on λ_T . A more detailed discussion of the method used to compute ϕ and \bar{w}_{ext} is delayed until the end of this section.

The stack placement in the resonance tube for minimum onset temperature gradient can be determined by the additional condition that τ be minimized with respect to phase angle. The phase angle for minimum onset temperature gradient, with the assumption that \bar{w}_{ext} varies negligibly with z , is determined from

$$\tan(\phi_{\text{min}}) = \sqrt{\frac{(\gamma-1)\text{Im} F^*(\lambda_T) + \bar{w}_{\text{ext}}}{\text{Im} F^*(\lambda) |\Omega F(\lambda)|^2 + \bar{w}_{\text{ext}}}}. \quad (7)$$

The corresponding minimal nondimensional temperature gradient is given by

$$\tau_{\text{min}} = \frac{\Omega(1 - N_{\text{pr}})}{\text{Im}\{F^*(\lambda_T)/F^*(\lambda)\}} \sqrt{[(\gamma-1)\text{Im} F^*(\lambda_T) + \bar{w}_{\text{ext}}] [\text{Im} F^*(\lambda) |\Omega F(\lambda)|^2 + \bar{w}_{\text{ext}}]}. \quad (8)$$

Equations (7) and (8) illustrate the role played by the thermoviscous dissipation function $F(\epsilon)$ in thermoacoustics. When $\bar{w}_{\text{ext}} \gg 1$, $\phi_{\text{min}} = \pi/4$ and $\tau_{\text{min}} = (1 - N_{\text{pr}}) \bar{w}_{\text{ext}} \Omega / [\text{Im}\{F^*(\lambda_T)/F^*(\lambda)\}]$. In this case, the losses in the stack are much less than the acoustic load elsewhere so the stack is

to be positioned for maximum effectiveness of the thermoacoustic gain term, i.e., where the product of acoustic pressure and particle velocity are a maximum at a distance $\frac{1}{4}$ of the acoustic wavelength from the hot end. For an inviscid gas, $F(\lambda) = 1$, and for $\bar{w}_{\text{ext}} = 0$, there is no acoustic load and

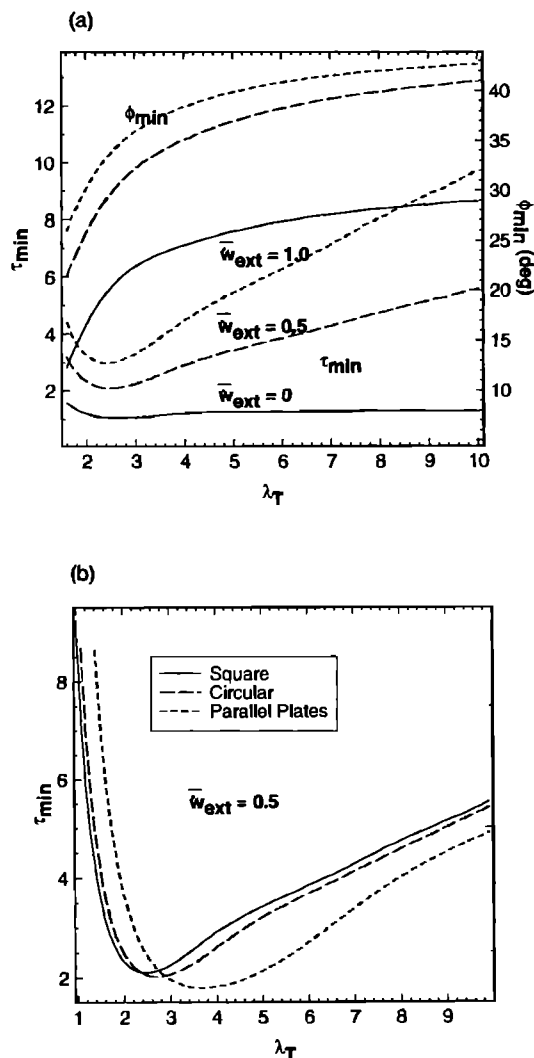


FIG. 4. (a) Normalized minimum onset temperature gradient and corresponding phase angle for the square pore geometry. Values of the external work load flow, \bar{w}_{ext} are 0 (solid), 0.5 (dashed), and 1 (shorter dashes) and are labeled on the τ_{min} curves. (b) Normalized minimum onset temperature gradient for the indicated pore geometries with same external work flow load $\bar{w}_{ext}=0.5$.

$\phi_{min} = \pi/2$. The stack is at the pressure node a distance of $\frac{1}{4}$ of an acoustic wavelength from the hot end. In a realistic engine the viscous losses in the stack and heat exchangers dominate, and the optimum stack position is displaced from $\pi/4$ toward the end of the tube. At this location the viscous losses are reduced. The value $\phi_{min} = 29.5$ deg computed for $\bar{w}_{ext} = 0.52$ appropriate for the experiment and for $\lambda_T = 2.4$ is in acceptable agreement with the value $\phi = 27.2$ deg determined from the accurate calculations described in Sec. III.

The normalized onset temperature gradient τ_{min} and corresponding phase angle ϕ_{min} are shown in Fig. 4(a) for a variety of external work loads for square pore stack geometry. Expressions for $F(\epsilon)$ for the various geometries are given in Ref. 4. Porosity $\Omega = 0.69$ was used in the calculations. The value of λ_T for optimal (lowest value) τ_{min} depends on the external work load. As \bar{w}_{ext} increases, τ_{min} increases, and $\phi_{min} \rightarrow \pi/4$ deg. Figure 4(b) shows τ_{min} for a variety of pore geometries at a constant external work load. Note that the parallel plate geometry gives lower τ_{min} than

the others. Swift and Keolian¹³ have shown that convex pore, pin array stacks have theoretical figures of merit for thermoacoustic refrigeration greater than all of the previously studied concave pore geometries. It is anticipated that pin array stacks should also have lower τ_{min} than the concave pore geometries, and the transition geometry of parallel plates.

The short stack approximation given above is inherently flawed because it assumes a constant value of λ_T in the stack. However, the approximation produces surprising agreement between theory and experiment, and much physical insight.

Our method is now described in greater detail for computing \bar{w}_{ext} and ϕ from an accurate calculation as described in Sec. III. In Ref. 4 it was shown that work flow is computed from $\bar{W}_2(z)/A_{res} = |P_1(z)^2 \text{Re } Z(z)/[2|Z(z)|^2]$, where $Z(z)$ is specific acoustic impedance and $P_1(z)$ is acoustic pressure. Work flows out of both ends of an operating time prime mover to supply acoustic power for resonator and heat exchanger losses and acoustic loads. Work flow is thus positive at one end of the stack, and negative at the other. The external work flow \bar{w}_{ext} is just the sum of the absolute value of the work flow at the ends of the stack. There exists an intermediate point z_1 in the stack defined by the condition $\bar{W}_2(z_1) = 0$. Note $\text{Re } Z(z_1) = 0$ at the intermediate point so that pressure and particle velocity have true standing wave phasing, i.e., they are out of phase by $\pi/2$. The phase angle at the intermediate point is

$$\tan \phi(z_2) = -i\rho_0 c/Z(z_2), \quad (9)$$

where ambient density ρ_0 and adiabatic sound speed c are to be evaluated at the intermediate temperature T_1 . This equation applies only at the intermediate point where Z is purely imaginary, and was motivated by Eqs. (2a)–(2c). The phase angle can also be estimated for arbitrary z by $\cos \phi(z) = \text{Re}\{P_1(z)/P_1(0)\}$. The onset condition given in Eq. (4) is evaluated at the intermediate point.

IV. CONCLUSIONS

A thermoacoustic prime mover was designed, constructed, and tested to probe the relation between thermal boundary layer thickness and onset temperature in a thermoacoustic engine. The stack had walls that were porous as well. Theoretical analysis indicates accuracy better than 2% in predicting the onset temperature difference and frequency of operation for the prime mover. The short stack approximation was used to derive expressions for the normalized onset temperature gradient and optimal stack location, yielding agreement with experiment to better than 6%. The minimum normalized onset temperature gradient was computed for three concave pore geometries and the results suggest that parallel plates are a better choice than either square or circular pore geometries. The short stack results should be useful in searching for efficient heat driven refrigerators and prime movers.

ACKNOWLEDGMENTS

This work was supported by the Office of Naval Research.

- ¹M. R. Stinson, "The propagation of plane sound waves in narrow and wide circular tubes, and generalization to uniform tubes of arbitrary cross-sectional shape," *J. Acoust. Soc. Am.* **89**, 550–558 (1991).
- ²N. Rott, "Thermoacoustics," *Adv. Appl. Mech.* **20**, 135–175 (1980).
- ³G. W. Swift, "Thermoacoustic engines," *J. Acoust. Soc. Am.* **84**, 1145–1180 (1988).
- ⁴W. P. Arnott, H. E. Bass, and R. Raspet, "General formulation of thermoacoustics for stacks having arbitrarily shaped pore cross sections," *J. Acoust. Soc. Am.* **90**, 3228–3237 (1991).
- ⁵T. von Hoffmann, U. Lienert, and H. Quack, "Experiments on thermally driven gas oscillations," *Cryogenics* **13**, 490–492 (1973).
- ⁶T. Yazaki, A. Tominaga, and Y. Narahara, "Stability limit for thermally driven acoustic oscillations," *Cryogenics* **19**, 393–396 (1979).
- ⁷H. S. Roh, W. P. Arnott, J. M. Sabatier, and R. Raspet, "Measurement and calculation of acoustic propagation constants in arrays of small air-filled rectangular tubes," *J. Acoust. Soc. Am.* **89**, 2617–2624 (1991).
- ⁸W. P. Arnott, J. M. Sabatier, and R. Raspet, "Sound propagation in capillary-tube-type porous media with small pores in the capillary walls," *J. Acoust. Soc. Am.* **90**, 3299–3306 (1991).
- ⁹W. P. Arnott, H. E. Bass, and R. Raspet, "Specific Acoustic Impedance measurements of an air filled prime mover," *J. Acoust. Soc. Am.* **92**, 3432–3434 (1992).
- ¹⁰J. C. Wheatley, "Intrinsically irreversible or natural engines," in *Frontiers of Physical Acoustics* (Tipografia Compositori, Bologna, 1986), p. 400.
- ¹¹A. D. Pierce, *Acoustics: An Introduction to Its Physic Principles and Applications* (American Institute of Physics, New York, 1989), p. 529.
- ¹²W. P. Arnott, R. Raspet, and H. E. Bass, "Thermoacoustic engines," *Proc. IEEE 1991 Ultrasonics Symp.* **2**, 995–1003 (1991). The last term of Eq. (6) should be $\text{Im} \{F^*(\lambda_T)/F^*(\lambda)\}$.
- ¹³G. W. Swift and B. Keolin, "Thermoacoustics in Pin-Array Stacks," *Acoust. Soc. Am.* **94**, 941–943 (1993).